Iterative Quantum-Assisted Multi-User Detection for Multi-Carrier Interleave Division Multiple Access Systems

Panagiotis Botsinis, *Student Member, IEEE*, Dimitrios Alanis, *Student Member, IEEE*, Zunaira Babar, *Student Member, IEEE*, Soon Xin Ng, *Senior Member, IEEE*, and Lajos Hanzo, *Fellow, IEEE*

***Abstract*—With the proliferation of smart-phones and tablet PCs, the data rates of wireless communications have been soaring. Hence, the need for power-efficient communications relying on low-complexity multiple-stream detectors has become more pressing than ever. As a remedy, in this paper we design low-complexity soft-input soft-output quantum-assisted multi-user detectors (QMUD), which may be conveniently incorporated into state-of-the-art iterative receivers. Our design relies on extrinsic information transfer charts. Our QMUDs are then employed in multi-carrier interleave-division multiple-access (MC-IDMA) systems, which are investigated in the context of different channel code rate and spreading factor pairs, whilst fixing the total bandwidth requirement. One of our QMUDs is found to operate within 0.5 dB of the classical maximum *a posteriori* probability MUD after three iterations between the MUD and the decoders, while requiring only half its complexity, at a BER of 10^{-5} in the uplink of a rank-deficient MC-IDMA system relying on realistic imperfect channel estimation at the receiver, while supporting 14 users transmitting QPSK symbols.**

***Index Terms*—Computational complexity, Dürr-Høyer algorithm, EXIT chart, Grover's quantum search algorithm, interleave division multiple access, multiuser detection, orthogonal frequency division multiplexing, quantum computing.**

List of Abbreviations

ACO	Ant Colony Optimization.
AE	Antenna Element.
AWGN	Additive White Gaussian Noise.
BBHT	Boyer-Brassard-Høyer-Tapp.
BER	Bit Error Ratio.
BS	Base Station.
CD	Classical Domain.
CF	Cost Function.
CFE	Cost Function Evaluation.
CSI	Channel State Information.
DES/DEC	DESpreader/DECoder.
DHA	Dürr-Høyer Algorithm.
DSS	Direct Sequence Spreading.
ETU	Extended Typical Urban.
EXIT	EXtrinsic Information Transfer.
FBKT	Forward & Backward Knowledge Transfer.
FD-CHTF	Frequency-Domain CHannel Transfer Function.
FFT	Fast Fourier Transform.
FKT	Forward Knowledge Transfer.
FW	Free Will.
IDMA	Interleave Division Multiple Access.
IFFT	Inverse Fast Fourier Transform.
MAA	MAximum Approximation.
MAP	Maximum *A posteriori* Probability.
MC	Multi-Carrier.
MI	Mutual Information.
ML	Maximum Likelihood.
MMSE	Minimum Mean Square Error.
MUA	MUlti-input Approximation.
MUD	Multi-User Detector.
NE	Neighbour Exploitation.
NSC	Non-Systematic Convolutional.
OFDM	Orthogonal Frequency Division Multiplexing.
QD	Quantum Domain.
QMUD	Quantum-assisted Multi-User Detection.
QSA	Quantum Search Algorithm.
QWSA	Quantum Weighted Sum Algorithm.
SF	Spreading Factor.
SISO	Soft-Input Soft-Output.
SO	Soft-Output.
SSCH	Slow SubCarrier Hopping.
USSCH	Uniform Slow SubCarrier Hopping.
ZF	Zero Forcing.

Manuscript received January 7, 2015; revised April 5, 2015 and June 5, 2015; accepted July 13, 2015. Date of publication July 21, 2015; date of current version October 15, 2015. The financial support of the European Research Council's Advanced Fellow Grant and of the Royal Society's Wolfson Reasearch Merit Award is gratefully acknowledged. The associate editor coordinating the review of this paper and approving it for publication was T. Q. S. Quek.

The authors are with the School of Electronics and Computer Science, University of Southampton, Southampton, SO17 1BJ, U.K. (e-mail: pb8g10@ecs.soton.ac.uk; da4g11@ecs.soton.ac.uk; zb2g11@ecs.soton.ac.uk; sxn@ecs.soton.ac.uk; lh@ecs.soton.ac.uk).

Digital Object Identifier 10.1109/TCOMM.2015.2458857

I. Introduction

THE number of users U that are supported by a single Base Station (BS) may be higher than the number of receive Antenna Elements (AE) at the BS, resulting in an uplink multiple-access system associated with a rank-deficient system matrix. The performance of low-complexity heuristic Multi-User Detectors (MUD) becomes inadequate in rank-deficient multiple-access systems [1]–[3]. Although the performance of the optimal Maximum *A posteriori* Probability (MAP) MUD may still remain adequate in rank-deficient systems, its

complexity is an exponential function of both the number of users U and of the number of bits per transmitted symbol.

Our motivation behind employing quantum-search aided MUD is that the globally optimal multi-level symbol, which minimizes our problem-specific Cost Function (CF), is found by an efficient search. In Soft-Input Soft-Output (SISO) MUD, only a limited subset of the best multi-level symbols having a near-optimum CF value has to be evaluated for achieving a near-optimal BER performance for the system [1]. At the same time, Quantum Search Algorithms (QSA), such as Grover's QSA [4], [5], the Boyer-Brassard-Høyer-Tapp (BBHT) QSA [6] and the Dürr-Høyer Algorithm (DHA) [7], have been shown to perform close to the optimal full search, while imposing a substantially lower number of CF Evaluations (CFE). Therefore, by employing the QSAs in the search problems that exist in the MUD procedures, we expect to improve the BER performance of a wireless communication system, despite reducing its complexity in terms of the number of CFEs required.

Due to space limitations, in this paper we will only briefly discuss the postulates of quantum computing, before delving into the analysis of Grover's QSA, as well as of the BBHT QSA and of the DHA. For an extensive tutorial on quantum computing, the motivated reader is referred to [8]–[10], as well as to Section V of [11] and to the tutorials included in Quantiki.[1] Moreover, for a tutorial on Grover's QSA, the reader may refer to [11], [12], while tutorials on both the BBHT QSA and on the DHA may be found in Section VI of [11]. Furthermore, tutorials on the application of quantum algorithms in multi-user detection are offered in [3], [11], [13].

As a benefit of exploiting the inherent parallelism of quantum computing [8]–[11], [14], Quantum-assisted MUDs (QMUD) may achieve a near-optimal performance even in rank-deficient systems, where conventional detectors, such as the Zero Forcing (ZF) aided and Minimum Mean Square Error (MMSE) detectors [1], as well as the Ant Colony Optimization (ACO) aided MUD [15], [16], fail to achieve near-optimal performance. Imre and Balazs proposed [17] a hard-output QMUD based on the Quantum Counting algorithm [6], [18]. In [11] we proposed a SISO QMUD based on the Quantum Weighted Sum Algorithm (QWSA) [11], [13], which is capable of achieving a Bit Error Ratio (BER) performance equivalent to that of the MAP MUD at a tunable complexity. In [2] we investigated a hard-output QMUD, which achieves the optimal Maximum Likelihood (ML) MUD's performance at a low complexity with the aid of the DHA [7]. In the same paper [2] we also proposed an early-stopping criterion for configuring the QMUD to operate within the affordable complexity budget. Finally, a number of low-complexity soft-output QMUDs adopting the MAximum Approximation (MAA) technique of [3], [15] and the MUlti-input Approximation (MUA) methodologies of [3], [16] were presented in [3]. These were found to be superior to the state-of-art ACO-aided MUDs [15], [16]. It should be noted that the QSAs [4], [6], [7], as well as the presented QMUDs mainly exploit the inherent parallelism and entanglement [8] of quantum computing, therefore they require a quantum computer for their operation. Hence we effectively simulate a quantum computer using a classical computer.

The Interleave Division Multiple Access (IDMA) scheme of [19]–[25] distinguishes the users supported with the aid of their unique, user-specific interleaving sequence, whilst each user employs the same channel code and the same Direct Sequence Spreader (DSS). These two procedures are combined in an IDMA system, which is achieved by swapping the position of the DSS and the interleaver of a classic CDMA system [26], which has the advantage of potentially increasing the performance of a CDMA system as a benefit of its increased diversity gain gleaned from the independently fading chips. After channel coding and spreading the information bit sequence, the users interleave their own resultant chip sequence with the aid of a uniquely allocated interleaving sequence. At the receiver, the MUD is invoked on a chip-by-chip basis by exploiting the user-specific channel impulse responses. Iterations between the MUD and the despreader-decoder (DES/DEC) may be performed for providing a better final estimate [27]. Finally, we consider Multi-Carrier (MC) IDMA owing to its increased flexibility, as detailed in [1], [26].

Given the aforementioned state-of-the-art, our novel contributions are:

1) Inspired by the Soft-Output (SO) QMUDs of [3], we propose the family of SISO DHA-MUA-aided QMUDs, which achieve a near-optimal performance even in rank-deficient systems with the aid of multiple MUD-(DES/DEC) iterations, whilst imposing a lower complexity than the SISO DHA-QWSA-aided QMUD of [11], [13]. We compare the SISO QMUDs to the optimal MAP MUD, as well as to the SO MMSE detector [1] and to a SISO ACO MUD, based on [3], [15], [16]. We also demonstrate that the family of DHA-MUA-aided QMUDs performs better than the DHA-MAA-assisted QMUDs in the context of iterative receivers.
2) We use EXtrinsic Information Transfer (EXIT) [28], [29] charts for designing the proposed QMUDs. When we use EXIT charts relying on the assumption that the MUD's output is Gaussian distributed [30], different conclusions are arrived at, depending on the associated simplifying assumptions.
3) The performance of the proposed QMUDs is evaluated in the context of novel MC-IDMA systems. By adjusting the values of the coding rate R and the Spreading Factor (SF) while keeping the R/SF ratio fixed, we evaluate their impact on the system's performance.
4) Finally, the effect of imperfect Channel State Information (CSI) on our SISO QMUDs and on the MAP MUD is investigated in the context of MC-IDMA systems.

This paper is structured as follows. In Section II we present the MC-IDMA system's model, while in Section III the necessary background on both quantum computing and on the QSAs employed is detailed. In Section IV we investigate the proposed SISO QMUDs, while in Section V we design them using EXIT charts. Moreover, in Section VI we employ the SISO QMUDs in the context of different MC-IDMA systems relying on both

[1] http://www.quantiki.org/wiki/Basic_concepts_in_quantum_computation

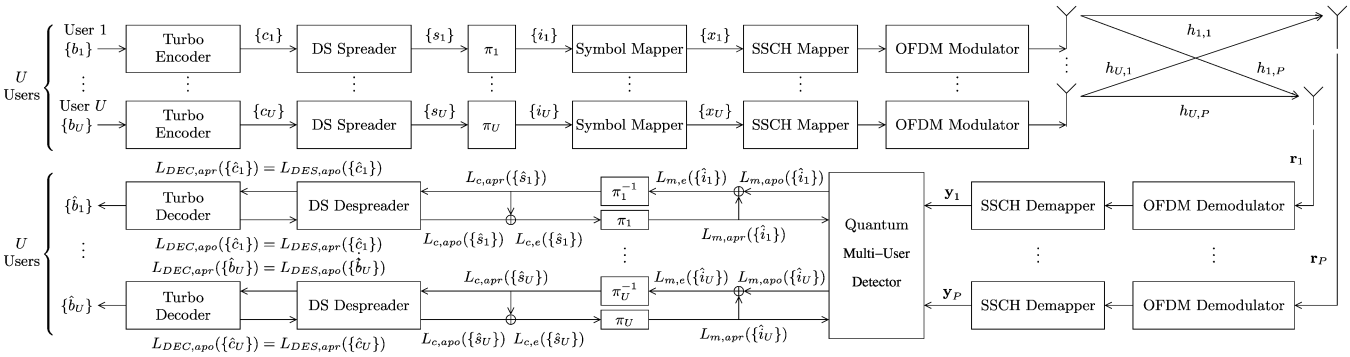

Fig. 1. MC-IDMA uplink communication system's block diagram supporting U users employing non-systematic convolutional coding and direct sequence spreading as well as iterative, soft-input soft-output QMUD at the BS.

perfect and imperfect CSI. Finally, our conclusions are offered in Section VII.

II. MC-IDMA System Model

Let us assume that U users are supported by our MC-IDMA system, as seen in Fig. 1. The uth user, $u = 1, 2, \ldots, U$, initially encodes his/her information bit sequence $\{b_u\}$ by a turbo encoder having a code rate R. The coded bit sequence $\{c_u\}$ of Fig. 1 is then spread using a DSS code having a spreading factor of SF. Since every user employs the same DSS code, this may be viewed as a repetition code having a code rate of $1/SF$ [30]. The turbo-encoded and DSS-spread bit sequence $\{s_u\}$ is then interleaved based on a user-specific interleaving sequence, resulting in the bit sequence $\{i_u\}$. Once the interleaved bit sequence of Fig. 1 has been mapped to symbols based on the M-ary modulation scheme selected and the symbol sequence $\{x_u\}$ has been obtained, it is mapped to the specific subcarriers that have been allocated to the uth user based on the Slow SubCarrier Hopping (SSCH) Mapper, followed by Orthogonal Frequency Division Multiplexing (OFDM) modulation by applying the classic Q-point Inverse Fast Fourier Transform (IFFT) of Fig. 1.

Let us also assume that the length of the symbol sequence $\{x_u\}$ is equal to Γ. Out of the Q available subcarriers of our system seen in Fig. 1 W subcarriers are allocated to each of the U users, obeying $W \leq Q$, $W \leq \Gamma$, mod $(\Gamma, W)=0$ and mod $(Q, W)=0$. In this treatise we apply the Uniform SSCH (USSCH) scheme [1] for allocating the subcarriers to the users. According to USSCH, the Q subcarriers are divided into W subbands having (Q/W) subcarriers in each subband as detailed in [3]. Following a subband-based allocation, each subcarrier is allocated to a randomly-selected user, until all the subcarriers of a subband have been allocated to a user or until there are no more users to be allocated, implying $U < Q/W$. Then, if $U > Q/W$, the same subcarriers are allocated to a second user, until all the subcarriers have been allocated to two users, or until all the users have been allocated to the subcarriers of that specific subband $(U < 2 \cdot Q/W)$. The same procedure continues, until all the users have been allocated to a subcarrier of that subband. An identical procedure applies to each subband. Eventually, the USSCH scheme creates a system where each subcarrier supports a similar number of users.

The U transmitted signals are received by the P receive AEs at the BS at the same time, assuming a synchronous system [1]. Therefore, at the pth receive AE, $p=1, 2, \ldots, P$, the U received signals are superimposed on each other, along with the Additive White Gaussian Noise (AWGN) having a zero mean and a variance of $N_0=2\sigma^2$. The resultant signal $\mathbf{r}_p=[r_{p,1}, r_{p,2}, \ldots, r_{p,Q}]^T$ is then OFDM demodulated by applying the Q-point Fast Fourier Transform (FFT) and dehopped according to the SSCH demapper, before $\mathbf{y}_p$ is forwarded to the MUD along with the rest of the signals gleaned from the other receive AE chains. The MUD operates on a subcarrier-basis. Let us focus our attention on the qth subcarrier and assume that the qth subcarrier has been allocated to U_q users, associated with $U_q < U$. The signal entering the MUD on the qth subcarrier is

$$\mathbf{y}_q = \mathbf{H}_q \cdot \mathbf{x}_q + \mathbf{n}_q, \tag{1}$$

where $\mathbf{y}_q=[y_{1,q}, y_{2,q}, \ldots, y_{P,q}]^T$ is the $(P\times 1)$-element received signal vector and $\mathbf{H}_q$ is the Frequency-Domain CHannel Transfer Function (FD-CHTF) on the qth subcarrier, which may be represented by a $(P\times U_q)$-element matrix as in

$$\mathbf{H}_q = \begin{bmatrix} h_{1,q}^{(1)} & h_{1,q}^{(2)} & \cdots & h_{1,q}^{(U_q)} \\ h_{2,q}^{(1)} & h_{2,q}^{(2)} & \cdots & h_{2,q}^{(U_q)} \\ \vdots & \vdots & \ddots & \vdots \\ h_{P,q}^{(1)} & h_{P,q}^{(2)} & \cdots & h_{P,q}^{(U_q)} \end{bmatrix}, \tag{2}$$

where $h_{p,q}^{(u_q)}$ is the complex-valued channel coefficient between the u_qth user and the pth receive AE on the qth subcarrier. Moreover, $\mathbf{x}_q=[x_q^{(1)}, x_q^{(2)}, \ldots, x_q^{(U_q)}]^T$ is the $(U_q\times 1)$-element symbol vector of the U_q users on the qth subcarrier and $\mathbf{n}=[n_{1,q}, n_{2,q}, \ldots, n_{P,q}]^T$ is the $(P\times 1)$-element noise vector.

The MAP MUD performs detection on a subcarrier basis by exploiting $\mathbf{y}_q$ from (1) and generates bit-based Log Likelihood Ratios (LLR). Focusing on the qth subcarrier supporting U_q users, the *a posteriori* bit based LLR of the u_qth user's mth bit at the output of the MAP MUD is formulated as

$$L_{m,po}\left(b_{u_q}^{(m)}\right) = \ln \frac{\sum_{\mathbf{x}\in\chi_q(u_q,m,0)} P\left(\mathbf{y}_q|\mathbf{x}\right) P(\mathbf{x})}{\sum_{\mathbf{x}\in\chi_q(u_q,m,1)} P\left(\mathbf{y}_q|\mathbf{x}\right) P(\mathbf{x})}, \tag{3}$$

where $\chi_q(u_q, m, \mathrm{v})$ is the set of legitimate multi-level symbols, which have the u_qth user's mth bit equal to v, with $u_q \in \{1, 2, \ldots, U_q\}$, $m \in \{1, 2, \ldots, \log_2(M)\}$ and $\mathrm{v} \in \{0, 1\}$. Furthermore, $P(\mathbf{y}_q|\mathbf{x})$ is the conditional probability of receiving the signal $\mathbf{y}_q$, given that $\mathbf{x}$ was transmitted. The product $f_{CF}(\mathbf{x})$ of the channel and of the *a priori* symbol probabilities $P(\mathbf{x})$ acts as our CF, which is equal to [30]

$$f_{CF}(\mathbf{x}) = \exp\left(-\left\|\mathbf{y}_q - \mathbf{H}_q\mathbf{x}\right\|^2 / 2\sigma^2\right) P(\mathbf{x}) = P\left(\mathbf{y}_q|\mathbf{x}\right) P(\mathbf{x}). \tag{4}$$

Finally, the *a priori* symbol probability $P(\mathbf{x})$ is fed back by the DES/DEC of Fig. 1 after having been appropriately rearranged by the interleaver π to the MUD as its extrinsic information, which is initially identical for all legitimate symbols $\mathbf{x}$. The extrinsic LLR at the output of the MUD of Fig. 1 is

$$L_{m,e}\left(b_{u_q}^{(m)}\right) = L_{m,po}\left(b_{u_q}^{(m)}\right) - \ln\frac{P\left(b_{u_q}^{(m)} = 0\right)}{P\left(b_{u_q}^{(m)} = 1\right)}. \tag{5}$$

As seen in Fig. 1, the bit-based extrinsic LLR stream of the uth user gleaned from all the W allocated subcarriers is deinterleaved based on the user-specific interleaver and then despread in the time domain, before it is fed to the turbo decoder, which outputs its own bit-based *a posteriori* LLRs. After a sufficiently high number of iterations between the MUD and the DES/DEC, a hard decision is made on the LLRs at the output of the decoder of Fig. 1, yielding the estimated $\{\hat{b}_u\}$ bit sequence.

III. Quantum Search Algorithms

The information unit in quantum computing is the quantum bit, or *qubit*.[2] A qubit $|q\rangle$ may be found in the quantum states $|0\rangle$, $|1\rangle$, or a superposition of these, as in $|q\rangle = a|0\rangle + b|1\rangle$, where $a, b \in \mathbb{C}$ and $|a|^2 + |b|^2 = 1$.[3] The probability of obtaining the state $|0\rangle$ upon observation of the qubit $|q\rangle$ is $|a|^2$, while that of obtaining the state $|1\rangle$ is $|b|^2$. The manipulation of a quantum state is performed by applying unitary operators to the qubits [9], with the most common one being the Hadamard operator H, which maps $H|0\rangle = (|0\rangle + |1\rangle)/\sqrt{2} = |+\rangle$ and $H|1\rangle = (|0\rangle - |1\rangle)/\sqrt{2} = |-\rangle$. Therefore, the Hadamard operator creates an equiprobable superposition of all legitimate states when the input qubit is in the $|0\rangle$ or $|1\rangle$ state, since $|a|^2 = |b|^2 = \left|\frac{1}{\sqrt{2}}\right|^2 = 0.5$. Quantum registers may be formed by employing n qubits and creating a superposition of up to 2^n states. Applying the Hadamard operator to 2 qubits in the zero state, would also yield an equiprobable superposition of all legitimate states, as in $|q_1\rangle|q_2\rangle = |q_1 q_2\rangle = H|0\rangle H|0\rangle = \left(\frac{|0\rangle+|1\rangle}{\sqrt{2}}\right)\left(\frac{|0\rangle+|1\rangle}{\sqrt{2}}\right) = 0.5|00\rangle + 0.5|01\rangle + 0.5|10\rangle + 0.5|11\rangle$. When two or more qubits' states cannot be described separately, for example when we have $|q_1 q_2\rangle = a|00\rangle + b|11\rangle$ for $n=2$, they are termed as being *entangled*, since a potential "measurement" or observation of one qubit affects the state of the other.[4]

Since in this treatise we only employ quantum algorithms that use real-valued amplitudes for the quantum states, we have $a, b \in \mathbb{R}$. Moreover, in an MC-IDMA system supporting U_q users on the qth subcarrier employing the classic M-ary multi-level modulation, there are M^{U_q} legitimate multi-level symbols. Let us represent each symbol by its decimal representation $x \in \{0, 1, \ldots, M^{U_q} - 1\}$. For example, if we have BPSK and $U_q = 2$, then $\mathbf{x} = [+1, -1]^T$ would be mapped to $x = [0, 1]_2 = 1_{10}$. Let us now present three QSAs, namely the Grover's QSA [4], [5], the BBHT QSA [6] and the DHA [7]. Our QMUDs employ the DHA a multiple number of times, which in turn make multiple calls to the BBHT QSA. The BBHT QSA is based on Grover's QSA, but it is capable of solving more general problems. An intuitive way of illustrating the employment of the quantum search algorithms in our QMUDs is depicted in Fig. 2, where the BBHT QSA and Grover's QSA are also included as a reference to the DHA.

A. Grover's Quantum Search Algorithm

Given a value δ and an N-element database representing a function $f(x)$ having N legitimate indices x, Grover's QSA [4], [5] was shown to be capable of finding that specific x value, for which we have $f(x) = \delta$ with $\sim$100% success probability after $O(\sqrt{N})$ database queries or function evaluations, where $O(\cdot)$ represents the order of a number. An entry in the database $f(x)$ that is equal to δ is hence referred to as a *solution*. In practical problems there may be several solutions and it is a prerequisite for the success of the search that the number of legitimate solutions S has to be known *a priori* in Grover's QSA [8], [9], [11].

Grover's QSA initializes $n = \log_2(N)$ qubits to the $|0\rangle^{\otimes n}$ state,[5] before passing them through a Hadamard gate, yielding

$$|x\rangle = \sum_{q=0}^{N-1} \frac{1}{\sqrt{N}}|q\rangle = \sum_{q=0}^{M^{U_q}-1} \frac{1}{\sqrt{M^{U_q}}}|q\rangle, \tag{6}$$

as detailed in [2]. This equiprobable superposition of $N = 2^n$ states is then fed to the Grover operator $\mathcal{G} = HP_0H \cdot O_{\mathcal{G}}$, where $O_{\mathcal{G}}$ is the Oracle operator, H is the Hadamard operator and P_0 is a rotation gate that maps $|0\rangle$ to $-|0\rangle$ and leaves all other states unaltered. The Oracle $O_{\mathcal{G}}$ marks those specific quantum states that correspond to the solutions found in the

[2]For an extensive tutorial on quantum computing and quantum search algorithms please refer to Sections V and VI of [11].

[3]A qubit $|q\rangle$ is in a superposition of two states $|0\rangle$ and $|1\rangle$, when the probability of observing it in one of these two states is not 100% [9].

[4]Two qubits are entangled when their quantum states cannot be described independently. Observation of an entangled qubit affects the quantum state of the unobserved qubit. For example, if we have two entangled qubits in the quantum state $|q_1\rangle|q_2\rangle = a|00\rangle + b|11\rangle$ and we obtain $|q_1\rangle = |0\rangle$ after its observation, then we may conclude that $|q_2\rangle$ is also $|0\rangle$ with 100% probability, without observing it.

[5]The n-element tensor product is defined as: $|0\rangle^{\otimes n} = \underbrace{|0\rangle_1 \otimes |0\rangle_2 \otimes \ldots \otimes |0\rangle_n}_{n} = \underbrace{|0\rangle_1|0\rangle_2 \ldots |0\rangle_n}_{n} = \underbrace{|00\ldots0\rangle}_{n}$.

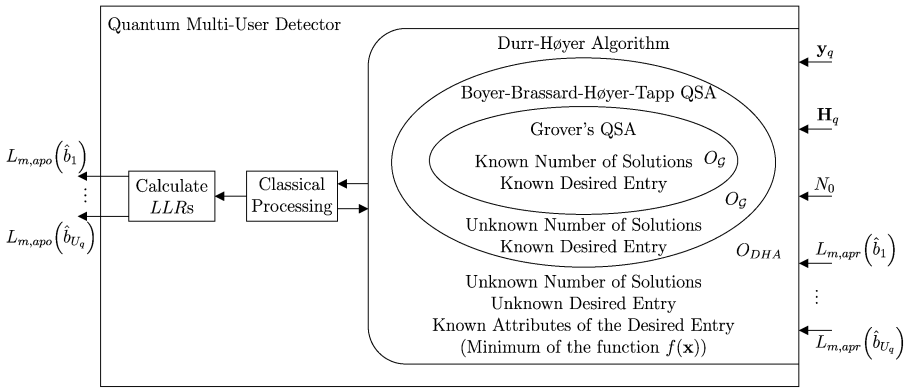

Fig. 2. The DHA employed in our QMUDs makes multiple calls to the BBHT QSA. Grover's QSA is not used, but it is included for terms of completion, since the BBHT QSA uses the same Oracle $O_{\mathcal{G}}$, but may even operate when the number of solutions is unknown. The QMUD is performed on a subcarrier basis. The DHA receives as input the received signals at all the receive AEs on the qth subcarrier, the channel estimates, the noise's variance and the *a priori* LLRs. After it completes its initial procedure, the DHA exchanges information with a classical processing unit, which determines whether the DHA should be called again and its search space. Finally, the QMUD outputs the calculated *a posteriori* LLRs.

database by flipping their polarity, essentially mapping $|x\rangle$ to $-|x\rangle$ if $f(x) = \delta$, by using an auxiliary qubit in the $|-\rangle$ state and evaluating f in parallel.[6] Since the actual complexity of the Oracle will depend on the particular technology used for creating the circuit, let us proceed by assuming that a single activation of the Oracle gate represents a single CFE [4], [6], [7], [9], [11]. The unitary operators HP_0H reflect the amplitude of each quantum state with respect to the average of the input amplitudes. Grover's operator $\mathcal{G}$ has to be applied to the state $|x\rangle$ in (6) $L_{opt} = \lfloor \pi/4\sqrt{N/S} \rfloor$ number of times. The probability of spotting one of the S solutions x, which satisfy $f(x) = \delta$, when observing the final state $\mathcal{G}^{L_{opt}}|x\rangle$ after L_{opt} applications of $\mathcal{G}$ is given by [5] $P_{success} = \sin^2[(2L_{opt} + 1)\theta]$, where we have $\theta = \arcsin(\sqrt{S/N})$.

B. The Boyer, Brassard, Hoyer, Tapp Quantum Search Algorithm

The Boyer-Brassard-Høyer-Tapp QSA [6] was termed after its inventors and it improves Grover's QSA by finding a solution x_s, where we have $f(x_s) = \delta$, with ∼100% success probability after $O(\sqrt{N})$ Oracle calls or CFEs, even when the number of solutions $S > 0$ is unknown. The BBHT algorithm employs Grover's operator $\mathcal{G}$ L times, where L is a pseudo-random number, to the equiprobable superposition of states, then measures or observes the resultant state $\mathcal{G}^L|x\rangle$ and if the observed state is not a solution, it restarts the procedure, as encapsulated in Fig. 3. Eventually, if we have $S > 0$ solutions, a solution x_s is found, or—alternatively—the BBHT QSA times out after $L^{QD}_{BBHT} = 4.5\sqrt{N/S}$ CFEs in the Quantum Domain (QD). A CFE in the Classical Domain (CD) is deemed to be completed,

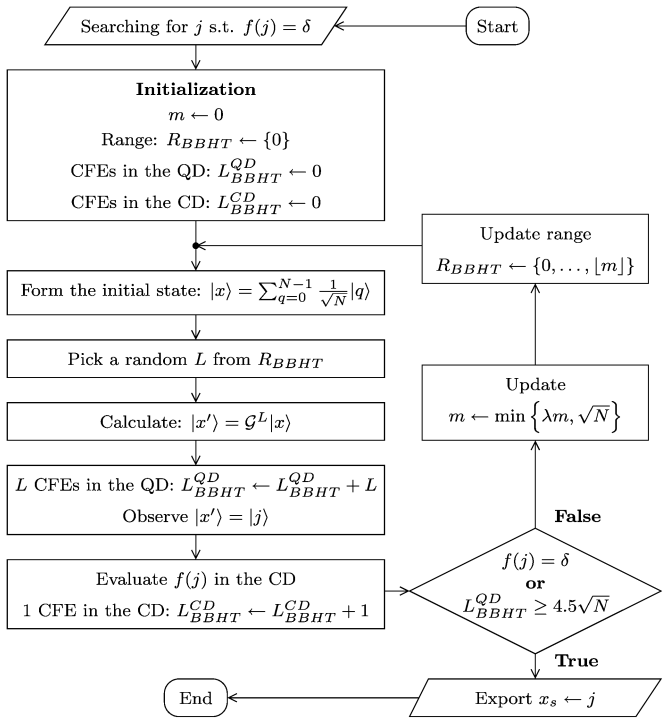

Fig. 3. Flow chart of the BBHT QSA.

when the observed state has been checked for being a solution. Since S is unknown, the selected time-out is set to correspond to the worst-case scenario of having only $S = 1$ solution, which corresponds to the highest possible number of CFEs given by:

$$L^{QD,\,\max}_{BBHT} = 4.5\sqrt{N}. \tag{7}$$

C. Dürr-Høyer Algorithm

As a further refinement, the DHA [7] employs the BBHT QSA in conjunction with its own specific Oracle operator O_{DHA} and succeeds in solving a different search problem, namely that of finding that specific $x_{\min}$, which minimizes a function

[6]Grover's Oracle [4] employs a unitary operator U_f, which evaluates the function f for all its inputs x simultaneously and saves the outputs $f(x)$ on auxiliary qubits, which were initially in the all-zero state [11]. For example, let us assume that f accepts single-bit inputs and the outputs are represented by two bits. If the input to U_f is $|q\rangle|00\rangle = a|0\rangle|00\rangle + b|1\rangle|00\rangle$, then U_f yields $U_f|q\rangle|00\rangle = a|0\rangle\underbrace{|f(0)\rangle}_{2} + b|1\rangle\underbrace{|f(1)\rangle}_{2}$.

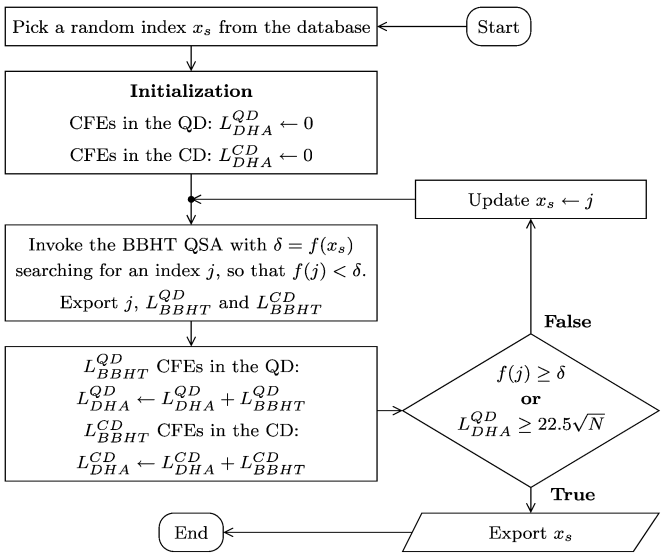

Fig. 4. Flow chart of the DHA.

$f(x)$ with ∼100% probability after $O(\sqrt{N})$ CFEs in both the QD and in the CD. The deterministically-initialized DHA's steps are summarized in Fig. 4. Commencing from an either randomly or deterministically selected value $f(x_s)$, we set $\delta = f(x_s)$. Then, the BBHT QSA is invoked by relying on a DHA-specific Oracle, which marks as solutions all those particular states that satisfy $f(x) < \delta$, by flipping their sign. After the BBHT operation has been completed, the function's value at the BBHT's output j is compared to δ. If we have $f(j) < \delta$, then x_s becomes equal to j and the BBHT is called again for $\delta = f(x_s)$. By contrast, if $f(j) \geq \delta$, it is concluded that there is no x satisfying $f(x) < \delta$ in the database, because the BBHT would have found it. Therefore, we accept that δ is the minimum value that $f(x)$ can have and the corresponding index of $x_{\min} = x_s$ represents the solution of the search problem considered. The maximum number of CFEs performed in the QD for the sake of finding the solution is $L_{DHA}^{QD,\max} = 22.5\sqrt{N}$ CFEs [3], [7], while the minimum number of the CD-CFEs is [3]

$$L_{DHA}^{CD,\min} = \min\left(L_{DHA}^{CD}\right) + 1$$
$$s.t. \left[\sum_{j=0}^{L_{DHA}^{CD}-1} \min\left(\left\lfloor \lambda^j \right\rfloor, \sqrt{N}\right)\right] \geq 4.5\sqrt{N}. \quad (8)$$

IV. Iterative Quantum Multi-User Detection

The families of DHA-MAA and DHA-MUA QMUDs were presented in [3], where they were employed in the context of non-iterative receivers. By contrast, here we investigate their behaviour, in the advanced context, when the system benefits from exchanging soft-information between the QMUD and the DES/DEC in the context of an attractive MC-IDMA system of Fig. 1. More specifically, the QMUDs perform approximations in the calculation of the bit-based LLRs of (3) and (5) for the sake of avoiding all M^{U_q} CFEs of the classical MAP MUD. However, the specific values of the extrinsic LLRs calculated at the output of the QMUD affect both the decoding procedure

TABLE I
Parameters of the 14-User MC-IDMA System

Number of Users	$U = 14$
Number of AEs per User	$N_{T_x} = 1$
Number of AEs at the BS	$P = 4$
Modulation	QPSK $M = 4$
Channel Code	Non-Systematic Convolutional Code, $R = 1/2$, 8 Trellis states
Spreading Factor	$SF = 2$
Number of Subcarriers	$Q = 1024$
Cyclic Prefix	CP = 128
Number of Subcarriers per User	$W = 512$
Normalized User Load	$U_L = U \cdot N_{T_x} \cdot W/(P \cdot Q) = 7/4$
Subcarrier Allocation every	$T_h = 5$ OFDM symbol periods
Bit Interleaver Length	20 480 per User
Channel Model	Extended Typical Urban (ETU) [31]
Mobile Velocity	$v = 130$ km/h
Sampling Frequency	$f_s = 15.36$ MHz
Carrier Frequency	$f_c = 2.5$ GHz
Normalized Doppler Frequency	$f_d = 1.96 \cdot 10^{-5}$
Channel Estimation	Perfect

and hence also the updated *a priori* probabilities $P(x)$. It is expected that if the QMUD outputs incorrect LLRs during the first QMUD-DES/DEC iteration, which we associate with erroneous signs or extremely high/low confidence, it will be difficult to correct them during the subsequent iterations, since the updated *a priori* LLRs will have been calculated based on these erroneous values. Therefore, we have to determine which approximations applied to the LLR calculations affect the suitability of the QMUDs to be implemented in iterative receivers and then compare the resultant QMUDs to the SISO DHA-QWSA QMUD proposed in [11], as well as to the MMSE MUD and to the proposed SISO ACO-based MUD, which is based on [3], [15], [16].

Let us focus our investigations on the uplink of the sophisticated MC-IDMA system of Fig. 1 supporting $U = 14$ users and transmitting QPSK symbols to $P = 4$ receive AEs. The system's parameters are summarized in Table I. We have selected a half-rate non-systematic convolutional (NSC) code and $SF = 2$ for the repetition-spreading code, resulting in a total code rate of $R_{total} = R/SF = 1/4$. The Extended Typical Urban (ETU) channel model of [31] corresponds to a high-velocity scenario, of $v = 130$ km/h, which we use for representing the maximum Doppler frequency for this channel model. We assume practical scenarios, where we experience complex-valued continuously fluctuating Rayleigh-fading envelopes at the subcarriers. Since the normalized Doppler frequency of the independent Rayleigh fading channels on each tap of the ETU channel model is equal to f_d and we have Q subcarriers, the effective Doppler frequency F_d becomes $F_d = Q \cdot f_d \simeq 0.02$. The normalized user load U_L is equal to 1.75, indicating a rank-deficient system, where conventional detectors would perform poorly. Since the $U = 14$ users transmit on half the subcarriers, we will have

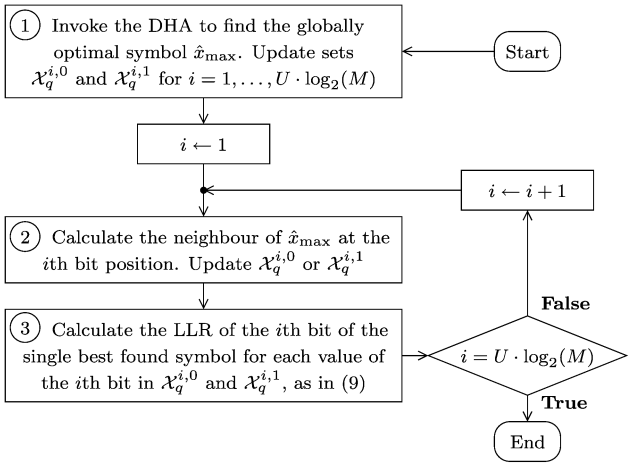

Fig. 5. Flow chart of the DHA-MAA-NE QMUD. In the DHA-MAA QMUD, Step 2 is ignored. A set $\mathcal{X}_q^{i,\nu}$ may also be represented as $\mathcal{X}_q^{u,m,\nu}$, where $i = (u-1) \cdot \log_2(M)+m$ and $\nu \in \{0, 1\}$.

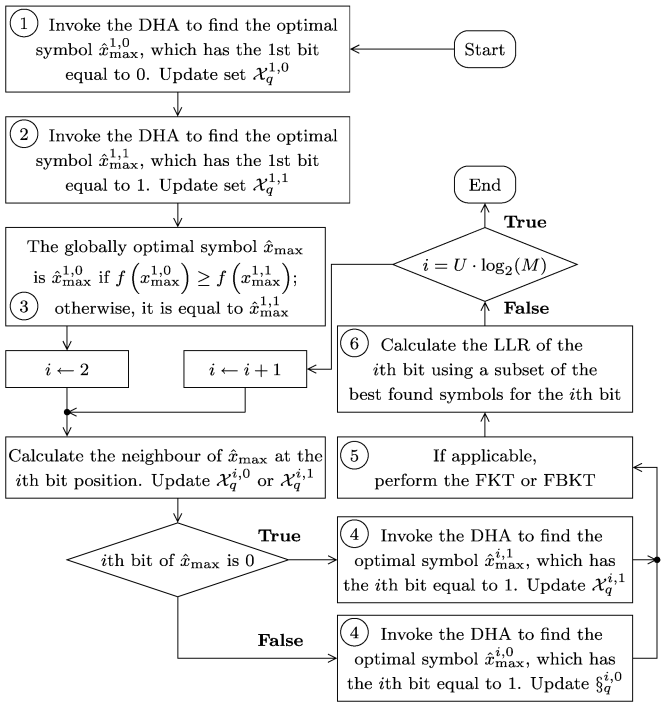

Fig. 6. Flow chart of the DHA-MUA QMUD. A set $\mathcal{X}_q^{i,\nu}$ may also be represented as $\mathcal{X}_q^{u,m,\nu}$, where $i = (u-1) \cdot \log_2(M)+m$ and $\nu \in \{0, 1\}$.

$U_q = 7$ for $q \in \{1, 2, \ldots, 1024\}$, allowing us to focus our discussions only on the qth subcarrier. Finally, the USSCH is applied every $T_h = 5$ OFDM symbol periods and every user transmits 10 240 symbols per frame.

The DHA-MAA QMUD [3] follows the procedure described in Fig. 5, while the DHA-MUA QMUD's [3] methodology is presented in Fig. 6. Once the sets $\mathcal{X}_q^{u,m,0}$ and $\mathcal{X}_q^{u,m,1}$ have been created for the $[(u-1) \cdot \log_2(M) + m]$th bit in the DHA-MAA QMUD, this bit's LLR is calculated based on [3]

$$L_{m,po}\left(b_u^{(m)}\right) = \ln \frac{\max\left(f(x)|x \in \mathcal{X}_q^{u,m,0}\right)}{\max\left(f(x)|x \in \mathcal{X}_q^{u,m,1}\right)}. \tag{9}$$

By contrast, in the DHA-MUA QMUD the LLR of the $[(u-1) \cdot \log_2(M) + m]$th bit is generated according to [3]

$$L_{m,po}\left(b_u^{(m)}\right) = \ln \frac{\sum\limits_{x \in \hat{\mathcal{X}}_q^{u,m,0}} f(x)}{\sum\limits_{x \in \hat{\mathcal{X}}_q^{u,m,1}} f(x)}. \tag{10}$$

The DHA-MAA QMUD performs a single DHA search in the set of all the legitimate multi-level symbols for finding the globally optimal symbol $\hat{x}_{\max}$ (Step 1 of Fig. 5) and it calculates the LLR of each bit based on the single best symbols evaluated for each bit's values in the process of finding $\hat{x}_{\max}$ (Step 3 of Fig. 5). The DHA-MUA QMUD calls the DHA twice for the first bit of the multi-level symbol—once for each of its binary values—searching for the optimal multi-level symbol of each value of the first bit (Steps 1 & 2 of Fig. 6). Therefore, the globally optimal symbol is decided to be that specific symbol, which has the higher CF value (Step 3 of Fig. 6). Afterwards, a single DHA search is performed for each remaining bit of the multi-level symbol fixing the Boolean value of that bit to the specific value, which is not part of the globally optimal symbol (Step 4 of Fig. 6). When the DHA-MUA QMUD relying on Forward Knowledge Transfer (FKT) [3] is used (Step 5 of Fig. 6), the respective sets of the subsequent bits, $b_{[(u-1)\cdot\log_2(M)+m+1]}, \ldots, b_{[U_q\cdot\log_2(M)]}$, are updated.[7] By contrast, for the DHA-MUA QMUD relying on Forward & Backward Knowledge Transfer (FBKT) [3] all the bits are updated.[8] The LLR of each bit is calculated based on the sets $\hat{\mathcal{X}}_q^{u,m,\nu} = \hat{\mathcal{X}}_q^{i,\nu}$, where we have $i = (u-1) \cdot \log_2(M)+m$ and $\nu \in \{1, 2\}$, which contain a selection of the best symbols in $\mathcal{X}_q^{i,\nu}$ [3]. More specifically, after sorting the entries of the sets for the ith bit based on their CF values, a pair of symbols is included in $\hat{\mathcal{X}}_q^{i,0}$ and $\hat{\mathcal{X}}_q^{i,1}$ from the sorted sets $\mathcal{X}_q^{i,0}$ and $\mathcal{X}_q^{i,1}$, provided that the LLR calculated solely on the basis of this pair of symbols would have the same hard decision as the globally optimal symbol $\hat{x}_{\max}$.

The BER performance of the DHA-MAA and DHA-MUA QMUDs employed in our MC-IDMA system described in Table I after 1, 2 and 3 MUD-DES/DEC iterations is presented in Fig. 7. The BER curves of the DHA-MUA QMUDs closely follow those of the MAP MUD, even when multiple MUD-DES/DEC iterations are employed, indicating that they are eminently suitable for iterative detection. On the other

[7] In the DHA-MUA QMUD, the search results obtained for the ith bit on the qth subcarrier are stored in $\mathcal{X}_q^{i,0}$ and $\mathcal{X}_q^{i,1}$. These search results are used only for calculating the LLR of the ith bit. When the Forward Knowledge Transfer modification is employed, the search results of the DHA related to the ith bit are also used for the calculation of the LLRs of the subsequent bits $b_{i+1}, b_{i+2}, \cdots, b_{[U\cdot\log_2(M)]}$ of the multi-level symbol, by being stored in their corresponding sets $\mathcal{X}_q^{i+1,0}, \mathcal{X}_q^{i+1,1}, \ldots, \mathcal{X}_q^{U\cdot\log_2(M),0}, \mathcal{X}_q^{U\cdot\log_2(M),1}$.

[8] Similarly to the Forward Knowledge Transfer modification, when the Forward & Backward Knowledge Transfer modification is employed, the search results of the DHA related to the ith bit are also used for the calculation of the LLRs of all the bits $b_1, b_2, \ldots, b_{[U\cdot\log_2(M)]}$ of the multi-level symbol, by being stored in their corresponding sets $\mathcal{X}_q^{1,0}, \mathcal{X}_q^{1,1}, \ldots, \mathcal{X}_q^{U\cdot\log_2(M),0}, \mathcal{X}_q^{U\cdot\log_2(M),1}$.

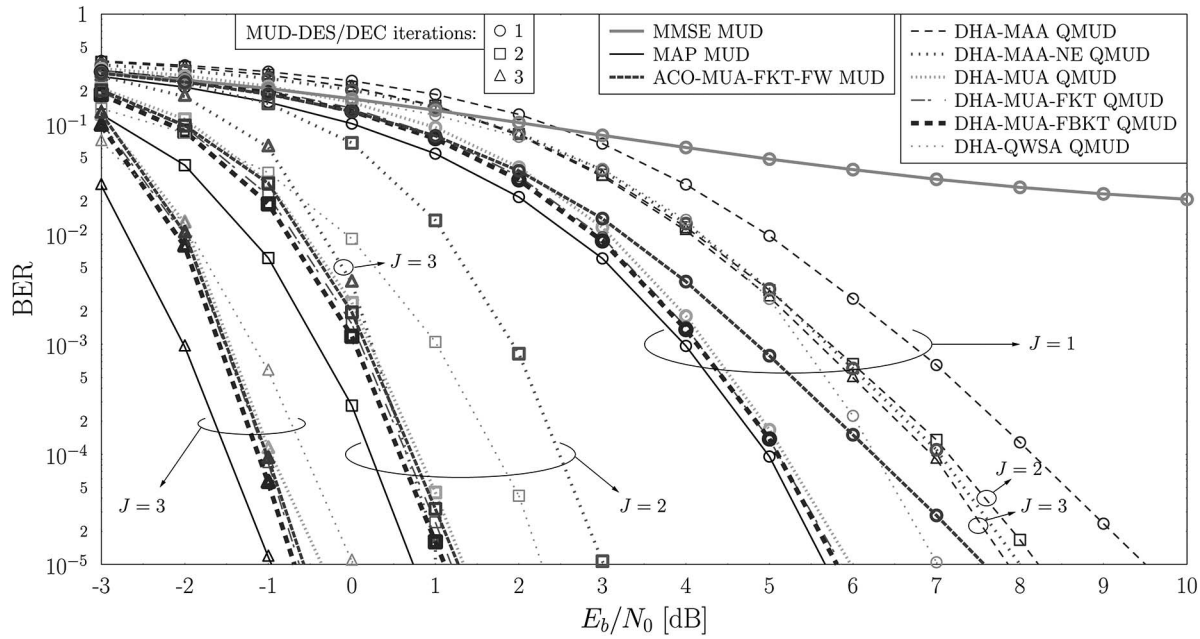

Fig. 7. BER performance of the families of DHA-MAA QMUDs and DHA-MUA QMUDs, as well as the MAP MUD, the ACO-MUA-FKT-FW MUD and the MMSE detector in the MC-IDMA system scenario of Table I. The ACO-MUA-FKT-FW MUD employed $\zeta = 18$ ants in $\Xi = 18$ generations during each search, the pheromone's weight was equal to $\alpha = 1$, the intrinsic affinity was equal to $\beta = 6$, the evaporation rate was equal to $\rho = 0.5$ and the free will probability was equal to $\mu_{FW} = 0.1$.

hand, we may observe that the performance of the DHA-MAA QMUDs is improved slower upon increasing the number of MUD-DES/DEC iterations. This is in contrast to the trend of both the MAP MUD and of the DHA-MUA QMUDs, both of which exhibit an approximately 5 dB improvement, when a second MUD-DES/DEC iteration is affordable. The DHA-MAA QMUD relying on Neighbour Exploitation (NE) [3] performs better than the DHA-MAA QMUD.[9] Quantitatively, it is only 2 dB away from the MAP MUD's curve at BER $= 10^{-5}$ after 3 MUD-DES/DEC iterations, compared to the 9 dB loss of the DHA-MAA QMUD. However, it still performs worse than the DHA-MUA QMUDs. Therefore, generating inflated LLRs based on the simplified LLR calculation of (9) for the DHA-MAA methodology results in lower-quality *a priori* LLRs at the output of the DES/DEC of Fig. 1. However, the DHA-MUA methodology, which uses the more accurate LLRs of (10) exhibits an improved BER in Fig. 7. The SISO DHA-MUA QMUDs also perform better than the DHA-QWSA QMUD with the aid of $l = 10$ control qubits, where the number of control qubits l in the DHA-QWSA QMUD determines both the precision of the LLRs' calculation, as well as the complexity of the QWSA as demonstrated in [11]. Explicitly, if we use more control qubits in the DHA-QWSA QMUD, the extrinsic LLRs will become more accurate, but the complexity will be higher.

We may observe that the MMSE detector characterized in Fig. 7 exhibits a BER floor at a BER of $\sim$0.02, which is due to the rank-deficient nature of the scenario. It is expected that in a system associated with a higher user load, the BER floor of the MMSE detector becomes even higher and it may appear at lower E_b/N_0 values. The fact that in the lower E_b/N_0 region of Fig. 7 the MMSE detector performs better than the DHA-MAA QMUD is related to the excessively high confidence erroneously provided by the DHA-MAA QMUD's extrinsic LLRs. Still referring to Fig. 7, we employed the SISO version of the ACO MUD relying on both the FKT and on Free Will (FW) [3] in conjunction with $\zeta = 18$ ants and $\Xi = 18$ generations during each ACO search.[10] The ACO-MUA-FKT-FW MUD performs worse than its quantum-aided counterpart, namely the DHA-MUA-FKT QMUD, during each MUD-DES/DEC iteration. For example, during the first MUD-DES/DEC iteration, there is an E_b/N_0 loss of 1.5 dB at a BER of 10^{-5}. During the second and third MUD-DEC/DEC iteration the E_b/N_0 loss becomes 0.085 dB and 0.055 dB, respectively. However, the complexity of the ACO-MUA-FKT-FW MUD is higher than that of the DHA-MUA-FKT QMUD during each MUD-DES/DEC iteration, suggesting that with the aid of the DHA-MUA-FKT QMUD we may be able to achieve a better performance at a reduced complexity. In systems having a normalized user-load of $U_L \geq 2$ the family of DHA-MUA QMUDs is expected to perform even better than that of the ACO-MUA MUDs and the MMSE detector, since its performance does not depend on the neighbourhood criterion.

[9]In the DHA-MAA QMUD, after the initial DHA search the sets $\mathcal{X}_q^{u,m,0}$ and $\mathcal{X}_q^{u,m,1}$ of each bit are updated with the search results, as in Step 1 of Fig. 5. Naturally, one of the two sets of each bit will include the globally optimal symbol $x_{\max}$. When the Neighbour Exploitation modification is employed, the set of each bit that does not include the globally optimal symbol $x_{\max}$ will include its neighbour symbol x_{nb} at that specific bit position, as described in Step 2 of Fig. 5, regardless of whether it is among the DHA's search results or not.

[10]The term *free will* may be considered as a bit-based mutation probability during the creation of a new ants' generation.

TABLE II
COMPLEXITY IN TERMS OF THE NUMBER OF CFEs/Bit IN FIG. 7

E_b/N_0	6 dB	1 dB	-1 dB
MUD-DES/DEC Iterations	1	2	3
MAP	1170	1170	1170
DHA-MAA	67	139	210
DHA-MAA-NE	68	140	213
DHA-MUA	744	1390	1998
DHA-MUA-FKT	599	1204	1773
DHA-MUA-FBKT	599	1204	1773
ACO-MUA-FKT-FW	649	1298	1947
DHA-QWSA	769	1472	2174

The complexities of the QMUDs employed are summarized in Table II. As expected, the complexities per bit of the QMUDs are lower than that of the MAP MUD during the first MUD-DES/DEC iteration. The number of CFEs/bit of the ACO-MUA-FKT-FW MUD is 8.35%, 7.81% and 9.81% higher than that of the DHA-MUA-FKT QMUD after the first, second and third MUD-DES/DEC iteration, respectively. When multiple MUD-DES/DEC iterations are used and we assume that perfect channel estimation is attainable before the first iteration with the aid of decision-directed channel estimation, then the complexity of the MAP MUD may remain constant, provided that we have sufficient memory for storing the CF values obtained during the first iteration. Naturally, in practical systems perfect channel estimation is unachievable, but a better channel estimate becomes available during each subsequent MUD-DES/DEC iteration, essentially forcing the MAP MUD to evaluate all the legitimate CF values again, hence resulting in 2340 and 3510 CFEs/bit after the second and third MUD-DES/DEC iteration, respectively. It is worth mentioning that according to Fig. 7 the DHA-MUA QMUDs outperform the DHA-QWSA QMUD associated with $l = 10$, despite requiring fewer CFEs/bit, as seen in Table II.

V. GAUSSIAN VERSUS NON-GAUSSIAN LLR DISTRIBUTIONS AND EXIT CHART ANALYSIS

Fig. 8 shows the EXIT chart of our system under the assumption of having a Gaussian distribution at the output of the DHA-MAA and DHA-MUA-FBKT QMUDs, as well as for the MAP MUD at $E_b/N_0 = 0$ dB. The reason that $E_b/N_0 = 0$ dB was selected for presenting the inner EXIT curves of the investigated QMUDs is that the EXIT chart design used in this paper is focused on a fixed-complexity system, where 3 MUD-DES/DEC iterations are allowed, rather than aiming for a near-capacity design, where the open tunnel area between the inner and outer EXIT decoder's curves should be as small as possible. Irregular convolutional codes [27], [28], [32] may be employed as outer codes in our system for exploiting their curve-matching capabilities to create a narrow but open tunnel between the inner and outer EXIT curves, hence achieving a near-capacity design. Therefore, for obtaining an infinitesimally low BER, the Monte-Carlo simulation based bit-by-bit decoding trajectory of the EXIT chart should reach the $I_{DES/DEC,e} = 1$ line after

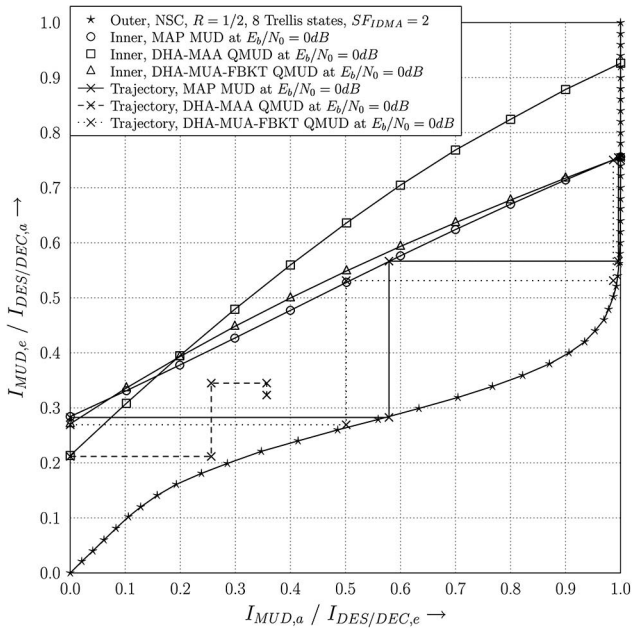

Fig. 8. EXIT chart of the DHA-MAA and DHA-MUA-FBKT QMUDs in the MC-IDMA system scenario of Table I. The inner and outer average EXIT curves of the MI are presented, along with the inner EXIT curves that take into consideration the standard deviation. Moreover, a snapshot of the inner EXIT curves and the corresponding trajectories are shown.

3 MUD-DES/DEC iterations. According to Fig. 7, both the MAP MUD, as well as the DHA-MUA, DHA-MUA-FKT, DHA-MUA-FBKT and the DHA-QWSA QMUDs exhibit a BER below 10^{-5} after 3 MUD-DES/DEC iterations, which is sufficiently low for cellular communications [1], at $E_b/N_0 = 0$ dB. Fig. 8 also includes the corresponding Monte-Carlo simulation based stair-case-shaped decoding trajectory where each user has transmitted a frame of 20 480 bits. Therefore, at $E_b/N_0 = 0$ dB we expect the decoding trajectory of the DHA-MUA-FBKT QMUD with an interleaver length of 20 480 bits per user to reach the $I_{DES/DEC,e} = 1$ line after 3 QMUD-DES/DEC iterations, as it is presented in Fig. 8.

According to Fig. 8, the QMUDs initially output a lower Mutual Information (MI) than the MAP MUD, but eventually "appear" to yield a higher MI. However, we will demonstrate that this fact does not represent the reality. To elaborate a little further, the investigated QMUDs always generate extrinsic LLRs, which have the same polarity as those of the MAP MUD. Due to the fact that the DHA-MAA QMUDs generate their LLRs according to (9) and that most of the time they do not use the optimal symbols—either for the numerator or for the denominator—we expected to obtain LLR values having the correct polarity, but a higher confidence than they should truly have. Therefore, their inner QMUD EXIT curves erroneously give the impression that the QMUDs outperform the MAP MUD.

Moreover, all the EXIT curves seen in Fig. 8 have been generated using Gaussian-distributed LLRs as their inputs, which is one of the necessary requirements to be satisfied for creating an accurate EXIT chart as a design tool [27]. In practice, this has been adopted because the outputs of both the widely used MUDs as well as of the channel decoders

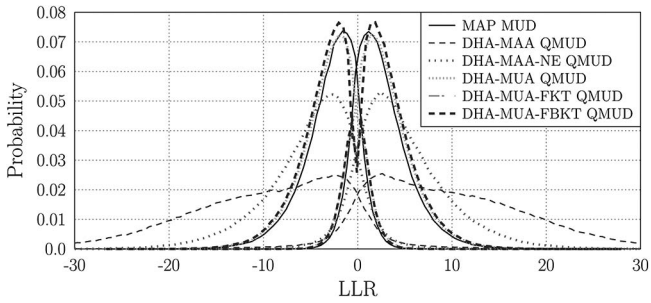

Fig. 9. Histograms of the output LLRs of the MAP MUD, the DHA-MAA, DHA-MAA-NE, DHA-MUA, DHA-MUA-FKT and DHA-MUA-FBKT QMUDs at $I_{MUD,a} = 0.5$ of a single frame of 20 480 bits per user in the system of Table I. The histograms which have their main peak at a positive LLR value correspond to the LLRs of a bit equal to 0, while those who have their main peak at a negative LLR value correspond to the LLRs of a bit equal to 1.

follow the Gaussian distribution, provided that their input is also Gaussian distributed. Since the initial input of the MUD obeys the Gaussian distribution with zero mean and zero standard deviation—this scenario corresponds to the $I_{MUD,a} = 0$ point—the generation of EXIT curves using input LLRs obeying the Gaussian distribution is indeed accurate. The output of the DHA-MUA QMUDs is also approximately Gaussian, but the actual output values of the DHA-MUA-FKT and DHA-MUA-FBKT QMUDs are slightly higher than those of the MAP MUD, as it may be observed in Fig. 9, where the PDF curves of the LLRs obtained for $I_{MUD,a} = 0.5$ are plotted. The DHA-MAA-NE QMUD mistakenly projects a higher confidence than that of the MAP MUD. By contrast, the DHA-MAA QMUD does not follow the Gaussian distribution and the probability of providing "over-confident" LLRs is expected to lead to a flawed design. More precisely, for $I_{MUD,a} = 0.5$ and for Gaussian distributed LLRs inputs to the MUDs, the probability of obtaining an LLR with an absolute value of $|L_{m,e}| \geq 5$ is 67.84% for the DHA-MAA QMUD, 21.98% for the DHA-MUA-FBKT QMUD and only 16.85% for the MAP MUD, indicating the excessive confidence exhibited by the QMUDs' outputs.

The histograms of the output LLRs of an MUD may be used for checking the consistency condition [33] for the eligibility of an MUD to be used in iterative receivers. More specifically, we may calculate the log-likelihood ratios of the bit-based LLRs of the *a posteriori* bit probabilities, based on their PDF curves shown in Fig. 9. If no approximations have been made in the calculations of the bit-based LLRs, we should expect the LLR values of the bit-based LLRs to be equal to those of the bit-based LLRs, therefore the corresponding curves seen in Fig. 10 should be on the main diagonal. Indeed, the MAP MUD's curve follows the main diagonal. Even though both the DHA-MAA and DHA-MUA QMUDs have relied on the approximations of (9) and (10), respectively, in the calculation of LLRs, the DHA-MAA QMUDs' curves are far away from the main diagonal in Fig. 10, due to their more crude approximation in (9), hence justifying the reduced gain achieved by allowing additional MUD-DES/DEC iterations, when compared to the rest of the MUDs.

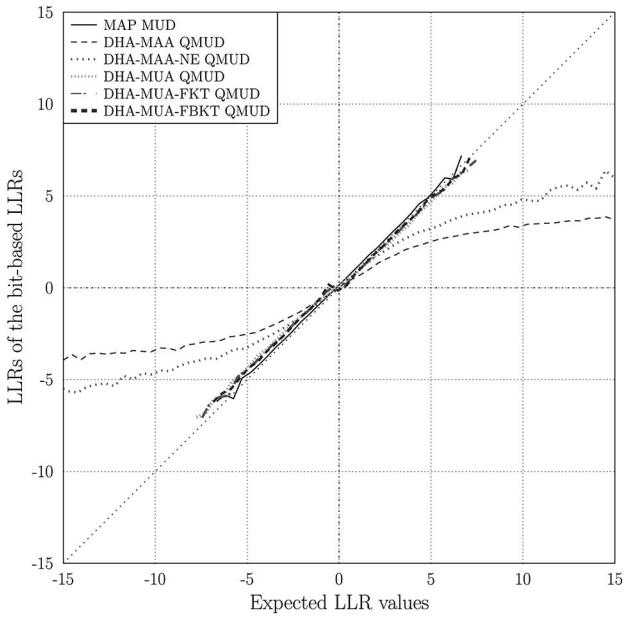

Fig. 10. LLR values obtained by the MUDs with respect to the expected LLR values based on the histograms in Fig. 9. The consistency condition for iterative detection for a particular MUD is satisfied if its corresponding curve is close to the main diagonal line. The frame length of each user is equal to 20 480 bits.

The fact that the inner detector EXIT curves generated with the aid of Gaussian assumptions correspond to an unrealistic scenario may be verified by inspecting the Monte-Carlo simulation based decoding trajectories of the QMUDs in Fig. 8, which do not accurately match the inner and outer decoder EXIT curves. The mismatch becomes particularly grave for the DHA-MAA QMUD, which exhibits a closed EXIT tunnel. Although not visible in Fig. 8, our investigations, which are included in the following figures, demonstrated that this mismatch occurs, because the inner and outer decoder EXIT curves that the system actually experiences during the second QMUD-DES/DEC iteration exhibit a lower MI than that shown by the EXIT curves generated with the aid of Gaussian assumptions, as a consequence of processing non-Gaussian distributed LLRs output by the previous MUD and DES/DEC processes. This is a result of the approximations applied in the calculations of the QMUD's LLRs in (9) and (10). For verifying the aforementioned speculations concerning the iterative behaviour of our proposed SISO QMUDs, let us now dispense with the assumption of having non-Gaussian LLRs in order to generate accurate EXIT charts [34] following the methodology described in Fig. 11, where two initialization stages are called. The number of initialization stages may be as high as required, with the first one being the same as the first stage in Fig. 11 and the rest being the same as the second stage in Fig. 11, incorporated right before the EXIT curve calculation stage. Again, in this paper we use up to two initialization stages.

An auxiliary $(E_b/N_0)^*$ value is selected during the initialization stages of Fig. 11. This $(E_b/N_0)^*$ value acts as our control parameter and replaces the need for having Gaussian distributed input LLRs corresponding to a specific $I_{MUD,a}$ value. Let us proceed by assuming that we only have a single initialization stage in Fig. 11 and that the 2nd initialization stage is

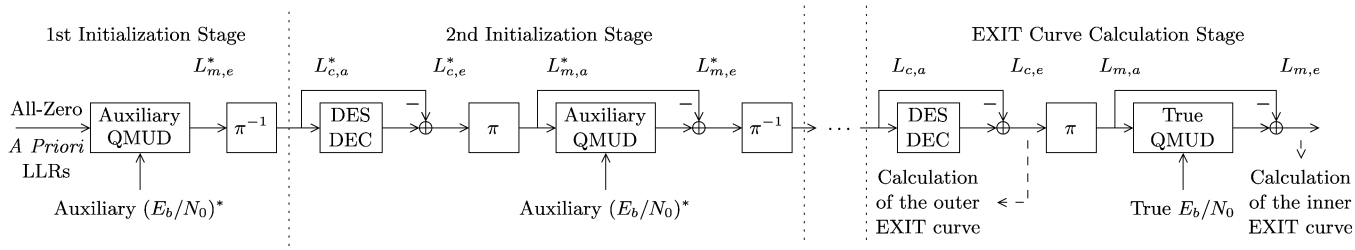

Fig. 11. Methodology for the generation of inner and outer EXIT curves with non-Gaussian distributed inputs by using two auxiliary MSDD-DEC iterations.

non-existent. By feeding the auxiliary QMUD with an all-zero *a priori* LLR sequence and the auxiliary $(E_b/N_0)^*$ value, at its output we obtain the auxiliary extrinsic LLRs $L^*_{m,e}$. These extrinsic LLRs obey the specific distribution, which characterizes the outputs of the auxiliary QMUD employed, and by calculating their MI after deinterleaving them, we are able to determine the specific $I_{DES/DEC,a}$ value of our non-Gaussian assumption-based EXIT chart. Still following Fig. 11 relying only on a single initialization stage, at the output of the DES/DEC used during the EXIT curve calculation stage we may obtain the extrinsic LLRs $L_{c,e}$, generated by a non-Gaussian input. Once we have calculated the corresponding MI of $L_{c,e}$, we have found the specific point $\{I_{DES/DEC,a}, I_{DES/DEC,e}\}$ of the EXIT outer curve. Moreover, the $L_{c,e}$ stream of Fig. 11 is interleaved and fed to the same QMUD, but operating at the true E_b/N_0 value we want to create the non-Gaussian inner EXIT curve for. At the output of the QMUD we may obtain the extrinsic LLRs, based on which we calculate $I_{MUD,e}$. By carefully tuning the auxiliary $(E_b/N_0)^*$ value, we are able to create the resultant inner and outer decoder EXIT curves. Let us assume now that both initialization stages are invoked in Fig. 11. We perform two MUD-DES/DEC iterations at the auxiliary $(E_b/N_0)^*$ value, commencing with an all-zero *a priori* LLR vector, before proceeding to the EXIT curve calculation stage. If the QMUDs affect the distribution of the output extrinsic LLRs, it is expected for the MI of both the inner and outer EXIT curves to have smaller values than those of the corresponding curves generated with none or a single auxiliary MSDD-DEC iteration. This would result in a narrower constriction in the open tunnel for the trajectory and it may explain why the trajectory of the DHA-MAA QMSDD seen in Fig. 8 gets stuck, despite having an open tunnel. Every initialization stage corresponds to an actual MUD-DES/DEC iteration of the decoding trajectory and an auxiliary MUD-DES/DEC iteration during the generation of the non-Gaussian PDF-based inner and outer decoder EXIT curves. Therefore, the trajectory is expected to match with the inner decoder's EXIT curve generated using 0 initialization stages during its first iteration, with the inner and outer EXIT curves generated using 1 initialization stage during its second iteration and so on.

The inner and outer decoder EXIT curves of the DHA-MAA QMUD with none, a single and two auxiliary MUD-DEC iterations are plotted for $E_b/N_0 = 0$ dB in Fig. 12, while those of the DHA-MUA-FBKT QMUD are presented in Fig. 13. The non-Gaussian inner and outer decoder EXIT curves were generated for $(E_b/N_0)^* = -3, -2, \ldots, 7$ dB. By observing the inner decoder's EXIT curve in both Figs. 12 and 13, we may conclude that for a fixed value of $I_{MUD,a}$, the

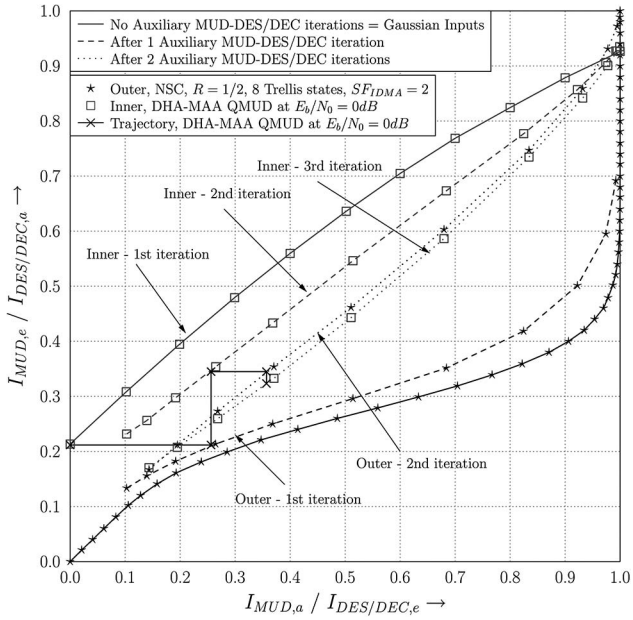

Fig. 12. EXIT chart of the DHA-MAA QMUD in the MC-IDMA system of Table I using 0, 1 and 2 auxiliary QMUD-DES/DEC iterations for the generation of the inner and outer EXIT curves for $E_b/N_0 = 0$ dB and $(E_b/N_0)^* = -3, -2, \ldots, 7$ dB. The inner and outer curves corresponding to each iteration match the decoding trajectory.

output MI of the DHA-MAA and DHA-MUA-FBKT QMUD becomes lower upon increasing the number of MUD-DES/DEC iterations, because the input and output LLRs do not obey the Gaussian distribution. Similarly, the same figures verify that the operation of the DES/DEC in Fig. 1 is also affected by the non-Gaussian LLR inputs. More specifically, the DES/DEC perturbs the classic turbo effect and provides a reduced $I_{DES/DEC,e}$ for the same $I_{DES/DEC,a}$ upon increasing the number of MUD-DES/DEC iterations, when the DHA-MAA QMUD is used. As expected for the DHA-MAA QMUD, the outer decoder's EXIT curve is above the inner decoder's EXIT curve after two MUD-DES/DEC iterations, essentially closing the tunnel. On the other hand, the trajectory of the DHA-MUA-FBKT QMUD shown in Fig. 13 can still get through the open tunnel after two iterations and reaches the $I_{DES/DEC,e} = 1$ line.

VI. Simulation Results and Discussions

The employment of non-Gaussian EXIT charts assists us in interpreting the exact behaviour of practical receivers, where approximations have been applied either at the MUDs or the

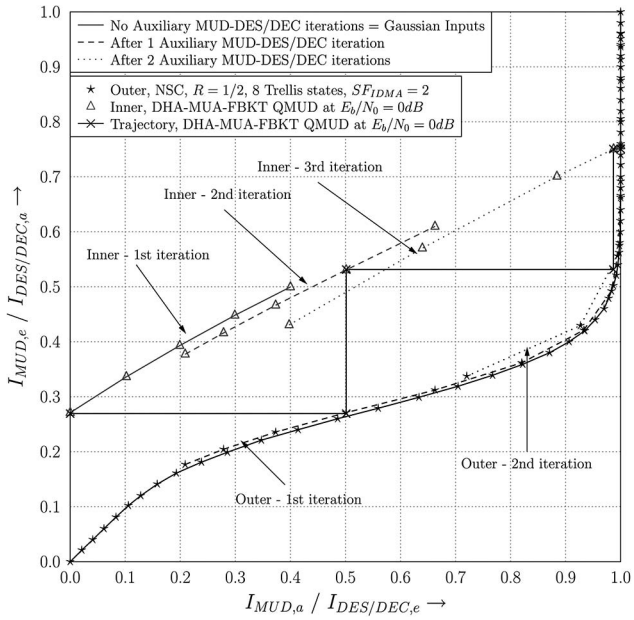

Fig. 13. EXIT chart of the DHA-MUA-FBKT QMUD in the MC-IDMA system of Table I using 0, 1 and 2 auxiliary QMUD-DES/DEC iterations for the generation of the inner and outer EXIT curves for $E_b/N_0 = 0$ dB and $(E_b/N_0)^* = -3, -2, \ldots, 7$ dB. Only the parts of the inner and outer EXIT curves that are in the proximity of the trajectory are shown for clarity.

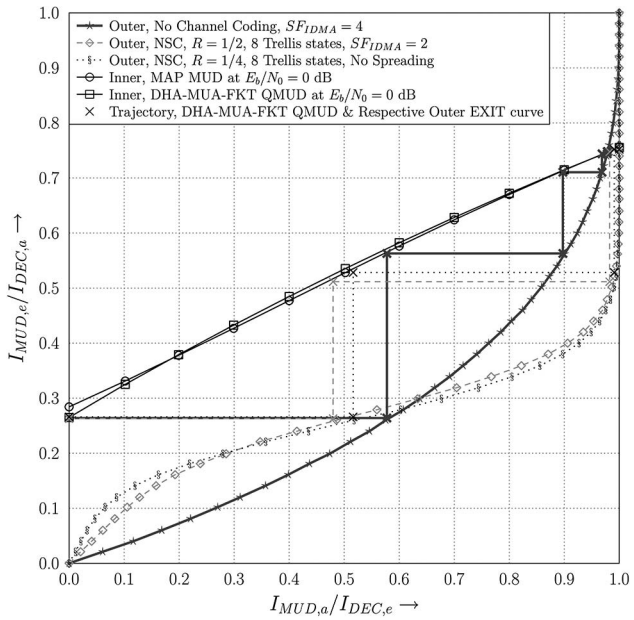

Fig. 14. EXIT chart of the DHA-MUA-FKT QMUD in 3 MC-IDMA system scenarios with $[R_1 = 1, SF_1 = 4]$, $[R_2 = 1/2, SF_2 = 2]$ and $[R_3 = 1/4, SF_3 = 1]$ and the rest of the parameters given in Table I.

decoders. However, since the DHA-MUA QMUDs are expected to have similar Gaussian and non-Gaussian EXIT charts, as shown in Fig. 8, in this section we will rely on Gaussian EXIT charts for characterizing the DHA-MUA-FKT QMUD.

Fig. 14 presents the EXIT chart of three MC-IDMA systems having $[R_1 = 1, SF_1 = 4]$, $[R_2 = 1/2, SF_2 = 2]$ and $[R_3 = 1/4, SF_3 = 1]$ and the parameters summarized in Table I. It should be noted that we have $R/SF = 1/4$ for all three systems,

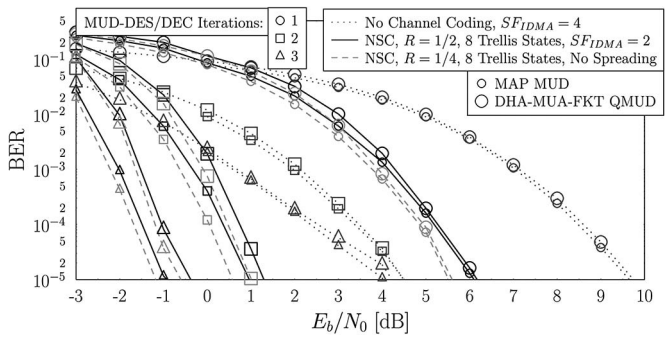

Fig. 15. BER performance of the DHA-MUA-FKT QMUD in 3 MC-IDMA system scenarios with $[R_1 = 1, SF_1 = 4]$, $[R_2 = 1/2, SF_2 = 2]$ and $[R_3 = 1/4, SF_3 = 1]$ and the rest of the parameters given in Table I.

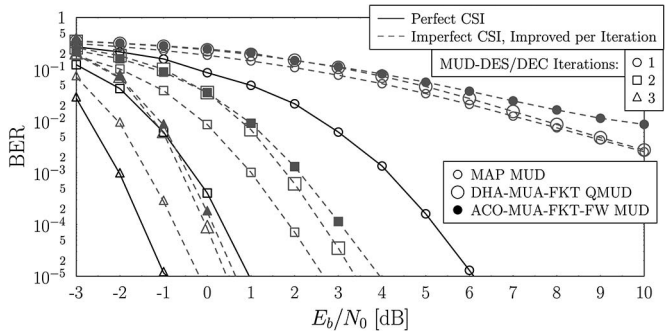

Fig. 16. BER performance of the DHA-MUA-FKT QMUD, as well as of the MAP and ACO-MUA-FKT-FW MUDs with $\zeta = 18$ ants and $\Xi = 18$ generations, in the system given in Table I with imperfect CSI, where $N_v = 0.0791, 0.0396, 0.0198$ during the first, second and third MUD-DES/DEC iteration.

therefore they have an identical throughput, since we keep the frame length the same. As expected, the inner decoder's EXIT curves which correspond to the MUD procedure are the same in all three systems. Based on the outer decoder's EXIT curves, the $[R_3 = 1/4, SF_3 = 1]$ system does not spread the bits and provides error-free decoding with the fewest iterations, provided that a sufficiently high E_b/N_0 value is used. In the other extreme scenario, the $[R_1 = 1, SF_1 = 4]$ system employs only a repetition code and performs better than the rest, when the power is so low that the EXIT tunnel will be closed for the $[R_2 = 1/2, SF_2 = 2]$ and $[R_3 = 1/4, SF_3 = 1]$ systems, even though it will not reach the $I_{DEC,e} = 1$ line. We may observe that even for $E_b/N_0 = 0$ dB, it outputs a higher MI than the other two systems during the first iteration. The $[R_2 = 1/2, SF_2 = 2]$ system's performance lies between that of the other two systems, but it is more similar to that of the $[R_3 = 1/4, SF_3 = 1]$ system. Based on Fig. 14, if the received power is high enough, we should expect a small difference between these two systems' performance. The conclusions we made based on the EXIT chart of Fig. 14 are verified by inspecting the BER vs E_b/N_0 curves encapsulated in Fig. 15, where we have invoked $J = 3$ MUD-DES/DEC iterations. The $[R_1 = 1, SF_1 = 4]$ system offers a lower BER at low powers, while the $[R_2 = 1/2, SF_2 = 2]$ and $[R_3 = 1/4, SF_3 = 1]$ systems perform equally well. However, the DES/DEC complexity of the $[R_2 = 1/2, SF_2 = 2]$ system is lower than that of the

TABLE III
SUMMARY OF THE PRESENTED QMUDS FOR THE MC-IDMA SYSTEM OF TABLE I AT BER $= 10^{-5}$

MUD	MUD-DEC iterations	Complexity (CFEs / bit)	% complexity of the MAP MUD	E_b/N_0 (dB)	E_b/N_0 difference from the MAP MUD (dB)
MAP	1	1170	100%	5.67	0
	2	1170	100%	0.74	0
	3	1170	100%	−0.96	0
DHA-MAA	1	67	5.7%	9.55	3.88
	2	139	11.9%	7.86	7.12
	3	210	17.9%	8.22	9.18
DHA-MAA-NE	1	68	5.8%	8.00	2.33
	2	140	12%	3.01	2.27
	3	213	18.2%	1.02	1.98
DHA-MUA	1	744	63.6%	5.97	0.3
	2	1390	118.8%	1.34	0.6
	3	1998	170.8%	−0.36	0.6
DHA-MUA-FKT	1	599	51.2%	5.86	0.19
	2	1204	102.9%	1.19	0.45
	3	1472	125.8%	−0.64	0.32
DHA-MUA-FBKT	1	599	51.2%	5.81	0.14
	2	1204	102.9%	1.15	0.41
	3	1472	125.8%	−0.69	0.27
ACO-MUA-FKT-FW	1	649	55.5%	7.57	1.9
	2	1298	110.9%	1.28	0.54
	3	1947	166.4%	−0.58	0.38
DHA-QWSA	1	769	65.7%	7.01	1.34
	2	1472	125.8%	2.27	1.53
	3	2174	185.8%	0.02	0.98

$[R_3 = 1/4, SF_3 = 1]$ system, even though they both use the same constraint length. This observation is due to having fewer coded bits at the output of the NSC and hence a reduced number of branches in the decoding trellis diagram [30], assuming that having 12 additional branches in a trellis diagram contributes more to the DES/DEC complexity than a half-rate repetition code does [30] in terms of the classic add-compare-select arithmetic operations.

In practice perfect CSI is not available, especially during the first MUD-DES/DEC iteration. For characterizing the systems, when only realistic imperfect CSI is available, we contaminated the perfect CSI values $h_{p,q}^{(u_q)}$ of (2) with AWGN, assuming that the CSI-estimation error is Gaussian, yielding

$$\tilde{h}_{p,q}^{(u_q)} = h_{p,q}^{(u_q)} + \nu, \tag{11}$$

where ν is an AWGN sample having a zero mean and a variance of N_ν, with $N_\nu = 0$ corresponding to the perfect CSI scenario. In our system we assume that the CSI noise power is halved during each MUD-DES/DEC iteration, modelling in this way the better CSI estimate that becomes available during each iteration. In Fig. 16 we have plotted the BER performance of the system characterized in Table I, when the DHA-MUA-FKT QMUD, as well as the MAP and ACO-MUA-FKT-FW MUDs with $\zeta = 18$ ants and $\Xi = 18$ generations are employed in conjunction with $N_\nu = 0.0791, 0.0396, 0.0198$ during the first, second and third iteration, respectively. We may observe that the DHA-MUA-FKT QMUD's performance is within 0.7 dB of that of the MAP MUD, regardless of the accuracy of the channel estimates, even though they are 6.5 dB away from the MAP MUD's performance recovered with the aid of perfect CSI at BER $= 0.0025$ after a single MUD-DES/DEC iteration. Furthermore, the DHA-MUA-FKT QMUD performs better than the ACO-MUA-FKT-FW MUD during all 3 MUD-DES/DEC iterations. An important observation is that with the aid of imperfect CSI, the MAP MUD has to repeat the CFEs during each MUD-DES/DEC iteration, in a similar way as the DHA-MUA-FKT QMUD, hence having completed in total 1170, 2340 and 3510 CFEs/bit after the first, second and third MUD-DES/DEC iteration, respectively, regardless of the power level and N_ν. At the same time, the DHA-MUA-FKT QMUD's complexity depends on both E_b/N_0 and on N_ν due to its deterministic initialization with the aid of the MMSE detector [3]. Therefore, assuming operation at BER $= 10^{-5}$ after $J = 3$ MUD-DES/DEC iterations, the DHA-MUA-FKT QMUD has carried out 600, 1226 and 1783 CFEs/bit, after the first, second and third MUD-DES/DEC iteration. At the same time, the ACO-MUA-FKT-FW has completed 649, 1298 and 1947 CFEs/bit, after the first, second and third MUD-DES/DEC iteration, regardless of the E_b/N_0 value.

Therefore, we may conclude that when the MAP MUD is called during each MUD-DES/DEC iteration, its complexity is higher than those of the proposed SISO QMUDs in a system having 2^{14} entries in its database. In fact, based on our simulations, the proposed SISO DHA-MAA and DHA-MUA QMUDs have a lower complexity than the MAP MUD, even when the database's size is reduced to 2^{12} entries, which corresponds to a scenario where 12 (3) users transmitting BPSK (16-QAM) symbols interfere with each other.

VII. Conclusion

Low-complexity SISO QMUDs were proposed and employed in MC-IDMA systems. In Fig. 7 we demonstrated that the family of DHA-MUA QMUDs is amenable to performing iterative detection, hence offering a near-optimal performance, approaching that of the MAP MUD, in contrast to the DHA-MAA. Furthermore, we concluded that all the proposed QMUDs perform better than the MMSE detector. The DHA-MUA-FKT QMUD was compared to the novel SISO ACO-MUA-FKT-FW MUD and it was found to exhibit an improved performance, despite imposing a reduced complexity. A summary of the BER performance and complexity of the employed MUDs with respect to the optimal MAP MUD is presented in Table III.

Since the inner EXIT curve analysis based on the Gaussian LLR distributions of the DHA-MAA QMUD seen in Fig. 8 is unable to plausibly explain the unsuitability of the DHA-MAA QMUD for employment in an iterative receiver, which is also evidenced by the decoding trajectory of Fig. 8, we presented an EXIT chart analysis based on non-Gaussian LLR distributions, which closely reflect the reality as it may be observed in Figs. 12 and 13. More precisely, the histogram-based EXIT charts with non-Gaussian *a priori* LLR distributions exhibit a more realistic scenario than the histogram-based EXIT charts with Gaussian *a priori* LLR distributions, since these specific *a priori* LLR distributions employed for the inner and outer decoder's EXIT curves are not randomly created following a Gaussian distribution, but instead they are the actual outcome of previous decoding and detection procedures. Therefore, EXIT charts based on non-Gaussian LLR distributions may provide a more accurate characterization of the iterative MUD-DES/DEC detection, when the MUD employed relies on simplifications, for example, when the reliability of calculating the LLRs based on a subset of all the legitimate multi-level symbols.

Moreover, in Figs. 14 and 15 we compared our MC-IDMA system to a pair of systems using either only NSC channel coding or DSS associated with the same joint coding rate of R/SF and with the same throughput, which was achieved by keeping the frame length the same. We may conclude that the system scenario associated with $[R_2 = 1/2, SF_2 = 2]$ is a better all-around choice for a system relying on $R/SF = 1/4$ specifications, since it performs almost equivalently to the $[R_1 = 1/4, SF_1 = 1]$ system, while imposing a lower decoding complexity.

Finally, for testing our QMUD in a practical system context, in Fig. 16 we evaluated the optimal MAP MUD, the ACO-MUA-FKT-FW MUD and the DHA-MUA-FKT QMUD in an MC-IDMA system, where only imperfect CSI was available, hence degrading the performance and forcing the MAP MUD to be employed during each MUD-DES/DEC iteration for exploiting the improved channel estimates. We may observe in Fig. 16 that the DHA-MUA-FKT QMUD continues to perform better than the ACO-MUA-FKT-FW MUD and near the optimal MAP MUD in terms of the system's BER versus the E_b/N_0 values, while only imposing about half the complexity after 3 MUD-DES/DEC iterations with respect to that of the MAP MUD, which is expressed in terms of the number of CFEs.

References

[1] L. Hanzo, Y. Akhtman, M. Jiang, and L. Wang, *MIMO-OFDM for LTE, WIFI and WIMAX: Coherent versus Non-Coherent and Cooperative Turbo-Transceivers*. Hoboken, NJ, USA: Wiley, 2010.

[2] P. Botsinis, S. X. Ng, and L. Hanzo, "Fixed-complexity quantum-assisted multi-user detection for CDMA and SDMA," *IEEE Trans. Commun.*, vol. 62, no. 3, pp. 990–1000, Mar. 2014.

[3] P. Botsinis, D. Alanis, S. X. Ng, and L. Hanzo, "Low-complexity soft-output quantum-assisted multiuser detection for direct-sequence spreading and slow subcarrier-hopping aided SDMA-OFDM systems," *IEEE Access*, vol. 2, pp. 451–472, 2014.

[4] L. K. Grover, "A fast quantum mechanical algorithm for database search," in *Proc. 28th Annu. ACM Symp. Theory Comput.*, Philadelphia, PA, USA, 1996, pp. 212–219.

[5] L. K. Grover, "Quantum mechanics helps in searching for a needle in a haystack," *Phys. Rev. Lett.*, vol. 79, no. 2, pp. 325–328, Jul. 1997.

[6] M. Boyer, G. Brassard, P. Høyer, and A. Tapp, "Tight bounds on quantum searching," *Fortschritte Phys.*, vol. 46, no. 4/5, pp. 493–506, 1998.

[7] C. Durr and P. Høyer, "A quantum algorithm for finding the minimum," Jul. 1996. arXiv:quant-ph/9607014.

[8] M. A. Nielsen and I. L. Chuang, *Quantum Computation and Quantum Information*. Cambridge, U.K.: Cambridge Univ. Press, 2000.

[9] S. Imre and F. Balázs, *Quantum Computing and Communications: An Engineering Approach*. Hoboken, NJ, USA: Wiley, 2005.

[10] S. Imre and L. Gyongyosi, *Advanced Quantum Communications: An Engineering Approach*. Hoboken, NJ, USA: Wiley, 2013.

[11] P. Botsinis, S. X. Ng, and L. Hanzo, "Quantum search algorithms, quantum wireless, and a low-complexity maximum likelihood iterative quantum multi-user detector design," *IEEE Access*, vol. 1, pp. 94–122, 2013.

[12] C. Williams, "Quantum search algorithms in science and engineering," *Comput. Sci. Eng.*, vol. 3, no. 2, pp. 44–51, Mar. 2001.

[13] P. Botsinis, S. X. Ng, and L. Hanzo, "Low-complexity iterative quantum multi-user detection in SDMA systems," in *Proc. IEEE ICC*, Sydney, Australia, 2014, pp. 5592–5597.

[14] D. Alanis, P. Botsinis, S. X. Ng, and L. Hanzo, "Quantum-assisted routing optimization for self-organizing networks," *IEEE Access*, vol. 2, pp. 614–632, 2014.

[15] C. Xu, B. Hu, L.-L. Yang, and L. Hanzo, "Ant-colony-based multiuser detection for multifunctional-antenna-array-assisted MC DS-CDMA systems," *IEEE Trans. Veh. Technol.*, vol. 57, no. 1, pp. 658–663, Jan. 2008.

[16] C. Xu, R. Maunder, L.-L. Yang, and L. Hanzo, "Near-optimum multi-user detectors using soft-output ant-colony-optimization for the DS-CDMA uplink," *IEEE Signal Process. Lett.*, vol. 16, no. 2, pp. 137–140, Feb. 2009.

[17] S. Imre and F. Balázs, "Non-coherent multi-user detection based on quantum search," in *Proc. IEEE ICC*, 2002, vol. 1, pp. 283–287.

[18] G. Brassard, P. Høyer, and A. Tapp, "Quantum counting," May 1998. arXiv:quant-ph/9805082.

[19] L. Ping, "Interleave-division multiple access and chip-by-chip iterative multi-user detection," *IEEE Commun. Mag.*, vol. 43, no. 6, pp. S19–S23, Jun. 2005.

[20] L. Ping, L. Liu, K. Wu, and W. K. Leung, "Interleave division multiple-access," *IEEE Trans. Wireless Commun.*, vol. 5, no. 4, pp. 938–947, Apr. 2006.

[21] R. Zhang and L. Hanzo, "Three design aspects of multicarrier interleave division multiple access," *IEEE Trans. Veh. Technol.*, vol. 57, no. 6, pp. 3607–3617, Nov. 2008.

[22] B. Cristea, D. Roviras, and B. Escrig, "Turbo receivers for interleave-division multiple-access systems," *IEEE Trans. Commun.*, vol. 57, no. 7, pp. 2090–2097, Jul. 2009.

[23] R. Zhang, L. Xu, S. Chen, and L. Hanzo, "EXIT-chart-aided hybrid multi-user detector for multicarrier interleave-division multiple access," *IEEE Trans. Veh. Technol.*, vol. 59, no. 3, pp. 1563–1567, Mar. 2010.
[24] H.-H. Chung, Y.-C. Tsai, and M.-C. Lin, "IDMA using non-gray labelled modulation," *IEEE Trans. Commun.*, vol. 59, no. 9, pp. 2492–2501, Sep. 2011.
[25] J. Dang, W. Zhang, L. Yang, and Z. Zhang, "OFDM-IDMA with user grouping," *IEEE Trans. Commun.*, vol. 61, no. 5, pp. 1947–1955, May 2013.
[26] L. Hanzo, L.-L. Yang, E.-L. Kuan, and K. Yen, *Single and Multi-Carrier DS-CDMA: Multi-User Detection, Space-Time Spreading, Synchronisation, Networking, and Standards*. Hoboken, NJ, USA: Wiley, 2003.
[27] L. Hanzo, O. Alamri, M. El-Hajjar and N. Wu, *Near-Capacity Multi-Functional MIMO Systems: Sphere-Packing, Iterative Detection and Cooperation*. Piscataway, NJ, USA: Wiley/IEEE Press, May 2009.
[28] M. El-Hajjar and L. Hanzo, "EXIT charts for system design and analysis," *IEEE Commun. Surveys Tuts.*, vol. 16, no. 1, pp. 127–153, 1st Quart. 2014.
[29] Z. Babar, S. Ng, and L. Hanzo, "EXIT-chart aided near-capacity quantum turbo code design," *IEEE Trans. Veh. Technol.*, vol. 64, no. 3, pp. 866–875, Mar. 2015.
[30] L. Hanzo, T. H. Liew, B. Yeap, R. Y. S. Tee, and S. X. Ng, *Turbo Coding, Turbo Equalisation and Space-Time Coding: EXIT-Chart Aided Near-Capacity Designs for Wireless Channels*. Hoboken, NJ, USA: Wiley, 2010.
[31] S. Sesia, I. Toufik, and M. Baker, *LTE, The UMTS Long Term Evolution: From Theory to Practice*. Hoboken, NJ, USA: *Wiley*, 2009.
[32] L. Hanzo, R. Maunder, J. Wang, and L. Yang, *Near-Capacity Variable-Length Coding: Regular and EXIT-Chart-Aided Irregular Designs*. Piscataway, NJ, USA: Wiley/IEEE Press, 2010.
[33] J. Hagenauer, "The EXIT chart—Introduction to extrinsic information transfer," in *Proc. 12th EUSIPCO Iterative Process.*, Vienna, Austria, 2004, pp. 1541–1548.
[34] Y.-M. Chen, Y.-L. Ueng, and H.-J. Shiau, "An exit-based design method for LDPC-coded schemes without Gaussian assumptions," *IEEE Communications Letters*, vol. 17, no. 8, pp. 1648–1651, Aug. 2013.

Panagiotis Botsinis (S'12) received the M.Eng. degree from the School of Electrical and Computer Engineering of the National Technical University of Athens (NTUA), Greece, in 2010, and the M.Sc. degree with distinction and the Ph.D. degree in wireless communications from the University of Southampton, U.K., in 2011 and 2015, respectively. He is currently working as a Research Fellow in the Southampton Wireless Group at the School of Electronics and Computer Science of the University of Southampton. Since October 2010, he has been a member of the Technical Chamber of Greece.

His research interests include quantum-assisted communications, quantum computation, iterative detection, OFDM, MIMO, multiple access systems, coded modulation, channel coding, cooperative communications, as well as combinatorial optimization.

Dimitrios Alanis (S'13) received the M.Eng. degree in electrical and computer engineering from the Aristotle University of Thessaloniki, Greece, in 2011, and the M.Sc. degree in wireless communications from the University of Southampton, U.K., in 2012. He is currently working towards the Ph.D. degree with the Southampton Wireless Group, School of Electronics and Computer Science, University of Southampton.

His research interests include quantum computation and quantum information theory, quantum search algorithms, cooperative communications, resource allocation for self-organizing networks, bio-inspired optimization algorithms, and classical and quantum game theory.

Zunaira Babar received the B.Eng. degree in electrical engineering from the National University of Science & Technology, Islamabad, Pakistan, in 2008, as well as the M.Sc. (Hons.) degree and the Ph.D. degree in wireless communications from the University of Southampton, U.K., in 2011 and 2015, respectively.

Her research interests include quantum error correction codes, channel coding, coded modulation, iterative detection, and cooperative communications.

Soon Xin Ng (S'99–M'03–SM'08) received the B.Eng. degree (first class) in electronics engineering and the Ph.D. degree in wireless communications from the University of Southampton, Southampton, U.K., in 1999 and 2002, respectively. From 2003 to 2006, he was a Postdoctoral Research Fellow working on collaborative European research projects known as SCOUT, NEWCOM, and PHOENIX. Since August 2006, he has been a member of academic staff in the School of Electronics and Computer Science, University of Southampton. He is involved in the OPTIMIX and CONCERTO European projects as well as the IU-ATC and UC4G projects. He is currently an Associate Professor of telecommunications with the University of Southampton.

He has authored over 180 papers and co-authored two John Wiley/IEEE Press books in his research field. His research interests include adaptive coded modulation, coded modulation, channel coding, space-time coding, joint source and channel coding, iterative detection, OFDM, MIMO, cooperative communications, distributed coding, quantum error correction codes, and joint wireless-and-optical-fiber communications. He is a Chartered Engineer and a Fellow of the Higher Education Academy in the U.K.

Lajos Hanzo (M'91–SM'92–F'04) received the First-class Master degree in electronics in 1976, the Ph.D. degree in 1983, and the Doctor Honoris Causa degree from the Technical University of Budapest in 2009. During the 37 years of career in telecommunications, he has held various research and academic positions in Hungary, Germany, and the U.K. Since 1986, he has been with the School of Electronics and Computer Science, University of Southampton, U.K., where he holds the Chair in Telecommunications. He has successfully supervised over 80 Ph.D. students, has co-authored 20 John Wiley/IEEE Press books in mobile radio communications totalling in excess of 10 000 pages, and authored over 1400 research entries at the IEEE Xplore. He has over 19 000 citations. He is a fellow of the Future Institute of Engineering and Technology, and the European Association for Signal Processing. He has acted as the TPC and General Chair of the IEEE conferences, presented keynote lectures, and received a number of distinctions. He is directing the 100-strong academic research team, working on a range of research projects in the field of wireless multimedia communications sponsored by the industry, the Engineering and Physical Sciences Research Council, U.K., the European Research Council's Advanced Fellow Grant, and the Royal Society's Wolfson Research Merit Award. He is an enthusiastic supporter of industrial and academic liaison, and offers a range of industrial courses. He is also a Governor of the IEEE Vehicular Technology Society. From 2008 to 2012, he was the Editor-in-Chief of the IEEE Press and a Chair Professor with Tsinghua University, Beijing. His research is funded by the European Research Council's Senior Research Fellow Grant.